Ultraslow light effect driven by quasibound states in the continuum in compound grating waveguide structures

Feng Wu[1,*] Xin Qi,[2] Ma Luo,[1] Tingting Liu,[3,4] and Shuyuan Xiao[3,4,†]

[1]*School of Optoelectronic Engineering, Guangdong Polytechnic Normal University, Guangzhou 510665, China*
[2]*MOE Key Laboratory of Advanced Micro-structured Materials, School of Physics Sciences and Engineering, Tongji University, Shanghai 200092, China*
[3]*Institute for Advanced Study, Nanchang University, Nanchang 330031, China*
[4]*Jiangxi Key Laboratory for Microscale Interdisciplinary Study, Nanchang University, Nanchang 330031, China*

(Received 10 July 2023; revised 25 September 2023; accepted 26 September 2023; published 4 October 2023)

Slow light effect plays a crucial role in both optical physics and devices. Herein, we explore the possibility to achieve ultraslow light effect based on the quasibound states in the continuum (quasi-BICs) in a compound grating waveguide structure. Driven by the unique resonant property of the quasi-BIC, the group velocity of light can be intensively slowed down to the order of $10^{-4}c$. Interestingly, we disclose that the group velocity of light and geometric perturbation parameters conforms to double-logarithm linear relationship. Our findings not only offer unique insight for the relation between slow light effect and BIC, but also provide a feasible route to achieving ultraslow light effect.

DOI: 10.1103/PhysRevB.108.165404

I. INTRODUCTION

Interaction between light and matter is a fundamental concept in optics [1,2]. It plays a crucial role in spontaneous emission [3], sensitive sensing [4,5], and cavity quantum electrodynamics systems [6–8]. In homogeneous media, large light speed gives rise to weak light-matter interaction [9]. In the past decades, researchers have found that light can be effectively slowed down in photonic crystals [10–14], cold gas vapors [15–18], and metamaterials [19,20]. Slow light effect promotes stronger light-matter interaction [21,22]. Consequently, slow light effect has been extensively utilized in delay lines [23,24], optical switchers [25,26], optical butters [27], enhancement of optical absorption [28,29], and enhancement of nonlinear optical effect [30]. Up until now, a series of mechanisms have been proposed to achieve slow light effect, including flat bands [31–36], electromagnetically induced transparency [37–42], plasmon-induced transparency [43–45], coherent population oscillations [46], stimulated Brillouin scattering [47], and stimulated Raman scattering [48]. Empowered by the above mechanisms, light speeds can be effectively slowed down to the order of 10^{-1} to $10^{-3}c$ [24,32,33,35,36,40,41]. Particularly, flat bands provide ultrahigh group indices but intensively compromise the bandwidths [31–36]. To broaden the bandwidths, researchers proposed the semislow light approach [49,50].

As a kind of resonant state, bound states embedded in continuous spectra called bound states in the continuum (BICs) have received abundant attention in nanophotonics [51–55]. After introducing perturbations, true BICs with infinite high-quality (Q) factors become quasi-BICs with finite high-Q factors [56]. Over the past two decades, many nanostructures have been proposed to realize quasi-BICs, including photonic crystal slabs [56–58], metasurfaces [59–65], and grating-based structures [66–74]. Particularly, researchers realized quasi-BICs in compound grating waveguide structures based on selectable guided resonances [75–78]. Recently, this kind of quasi-BICs demonstrated its potential applications in enhancement of spatial shift of light beam [75–77,79–81], enhancement of second-harmonic generation [82–84], and ultralow-threshold optical bistability [85]. In this paper, we explore the possibility to achieve ultraslow light effect based on this kind of quasi-BIC. Driven by the unique resonant property of the quasi-BICs in the compound grating waveguide structures, the group velocity of light can be intensively slowed down to the order of $10^{-4}c$. More interestingly, the group velocity of light v_g and geometric perturbation parameter α conforms to double-logarithm linear relationship, i.e., $\lg(v_g/c) = 2.0057\lg(\alpha) - 2.0133$. These results not only offer unique insight for the relation between slow light effect and BIC, but also provide a feasible route to achieving ultraslow light effect.

This paper is organized as follows. In Sec. II, we discuss BICs and quasi-BICs in a compound grating waveguide structure consisting of a four-part period grating and a waveguide layer based on the selectable guided resonance. As the geometric perturbation parameter changes from nonzero to zero, the four-part period grating turns into a conventional two-part period grating. Hence, the previous excitable odd-order guided resonances turn into dark modes, i.e., BICs. In Sec. III, we explore the relationship between the group velocity of light and geometric perturbation parameters. Interestingly, the group velocity of light and geometric perturbation parameters conforms to double-logarithm linear relationship. Finally, the conclusion is given in Sec. IV.

*fengwu@gpnu.edu.cn
†syxiao@ncu.edu.cn

 ©2023 American Physical Society

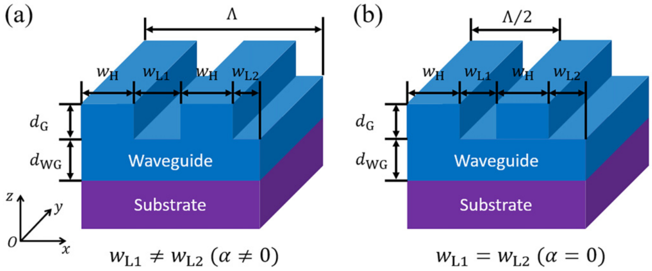

FIG. 1. Schematics of unit cells of compound grating waveguide structures for (a) $\alpha \neq 0$ and (b) $\alpha = 0$.

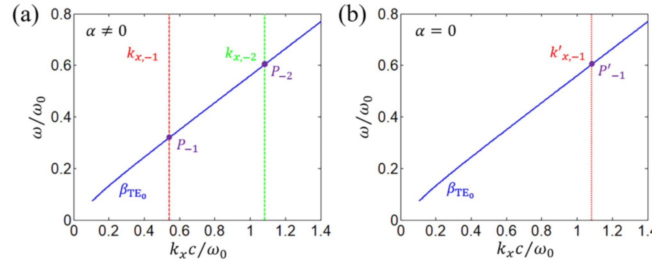

FIG. 2. GMRs in compound grating waveguide structures for (a) $\alpha \neq 0$ and (b) $\alpha = 0$.

II. BICS AND QUASI-BICS IN COMPOUND GRATING WAVEGUIDE STRUCTURES

The designed compound grating waveguide structure consisted of a four-part period grating, a waveguide layer, and a substrate. The period and thickness of the four-part period grating layer were chosen to be $\Lambda = 850$ nm and $d_G = 270$ nm, respectively. Two ridges were made of hafnium dioxide (HfO_2) with the refractive index $n_H = 1.88$ [86], while two grooves were made of air with the refractive index $n_L = 1$. The widths of the two HfO_2 ridges were both chosen to be $w_H = f_H\Lambda = 0.3\Lambda$. To form a complex lattice, the widths of the two air grooves were chosen to be $w_{L1} = f_{L1}\Lambda$ and $w_{L2} = f_{L2}\Lambda$, respectively. A geometric perturbation parameter $\alpha = (w_{L1} - w_{L2})/(w_{L1} + w_{L2})$ was defined to quantify the width difference between the two air grooves. As the geometric perturbation parameter $\alpha \neq 0$, the grating was a four-part period grating with the period $\Lambda = 850$ nm, as schematically shown in Fig. 1(a). The waveguide layer was also made of HfO_2 with the refractive index $n_{WG} = 1.88$ [86]. The thickness of the HfO_2 waveguide layer was chosen to be $d_{WG} = 460$ nm. The substrate was made of silicon dioxide (SiO_2) with the refractive index $n_S = 1.44$ [87]. As the geometric perturbation parameter $\alpha = 0$, the widths of the two air grooves become identical. Therefore, the grating turns into a conventional two-part period grating with the period $\Lambda' = \Lambda/2 = 425$ nm, as schematically shown in Fig. 1(b).

Then, we analyzed the guided-mode resonances (GMRs) for $\alpha \neq 0$ and $\alpha = 0$. Suppose that a plane wave with transverse electric (TE) polarization perpendicularly launches onto the compound grating waveguide structure at the xOz plane. According to the slab-waveguide theory, the dispersion relation of the TE_0 guided mode $\beta_{TE_0}(\omega)$ can be calculated by the four-layer slab-waveguide model [79,88,89]:

$$d_{WG}\sqrt{k_0^2 n_{WG}^2 - \beta_{TE_0}^2(\omega)} = \arctan\left[\frac{\sqrt{\beta_{TE_0}^2(\omega) - k_0^2 n_S^2}}{\sqrt{k_0^2 n_{WG}^2 - \beta_{TE_0}^2(\omega)}}\right] + \arctan\left[\frac{\sqrt{\beta_{TE_0}^2(\omega) - k_0^2 n_{eff}^2}}{\sqrt{k_0^2 n_{WG}^2 - \beta_{TE_0}^2(\omega)}} p(\omega)\right], \quad (1)$$

where

$$p(\omega) = \tanh\left\{\operatorname{arctanh}\left[\frac{\sqrt{\beta_{TE_0}^2(\omega) - k_0^2 n_0^2}}{\sqrt{\beta_{TE_0}^2(\omega) - k_0^2 n_{eff}^2}}\right] + d_G\sqrt{\beta_{TE_0}^2(\omega) - k_0^2 n_{eff}^2}\right\}. \quad (2)$$

In Eqs. (1) and (2), $k_0 = \omega/c$ represents the wave number in air, and $n_{eff} = 2f_H n_H + (1-2f_H)n_L = 1.528$ represents the effective refractive index of the grating layer.

As the geometric perturbation parameter $\alpha \neq 0$, the grating was a four-part period grating with the period $\Lambda = 850$ nm. The GMR condition took the following form [88]:

$$k_{x,m} = -p\frac{2\pi}{\Lambda} = \beta_{TE_0}(\omega)\ (p = \pm 1,\ \pm 2, \ldots), \quad (3)$$

where $m \times (2\pi/\Lambda)$ represents the grating-induced tangential wave vector. According to Eqs. (1) and (2), we calculated the dispersion relation of the TE_0 guided mode, as depicted by the blue solid line in Fig. 2(a). The normalized angular frequency was $\omega_0 = 2\pi c/d_{WG}$. The cutoff angular frequency of the TE_0 guided mode was calculated as $\omega_{c,\,TE_0} = 0.0733\omega_0$ ($f_{c,\,TE_0} = 47.80$ THz). According to Eq. (3), we also calculated the dispersion relations $k_{x,-1}$ and $k_{x,-2}$, as depicted by the red and green dashed lines in Fig. 2(a), respectively. As demonstrated, two crossing points (marked by P_{-1} and P_{-2}) occurred at the angular frequencies $\omega_{-1} = 0.3219\omega_0$ ($f_{-1} = 209.9$ THz) and $\omega_{-2} = 0.6032\omega_0$ ($f_{-2} = 393.4$ THz), respectively. At these two angular frequencies, two Fano resonances occurred since the GMR conditions were satisfied.

As the geometric perturbation parameter $\alpha = 0$, the grating turns into a conventional two-part period grating with the period $\Lambda' = \Lambda/2 = 425$ nm. Consequently, the GMR condition takes the following form:

$$k'_{x,p'} = -p'\frac{2\pi}{\Lambda'} = -p'\frac{4\pi}{\Lambda} = \beta_{TE_0}(\omega)\ (p' = \pm 1,\ \pm 2, \ldots). \quad (4)$$

Combining Eqs. (3) and (4), the dispersion relations $k'_{x,p'}$ are identical with $k_{x,2p'}$ since the grating-induced tangential wave vectors double. For example, the dispersion relation $k'_{x,-1}$ is identical with $k_{x,-2}$, as shown by the red dotted line in Fig. 2(b). Consequently, only one cross point (marked by P'_{-1}) occurs at the angular frequencies $\omega'_{-1} = \omega_{-2} = 0.6032\omega_0$ ($f'_{-1} = f_{-2} = 393.4$ THz). At this angular

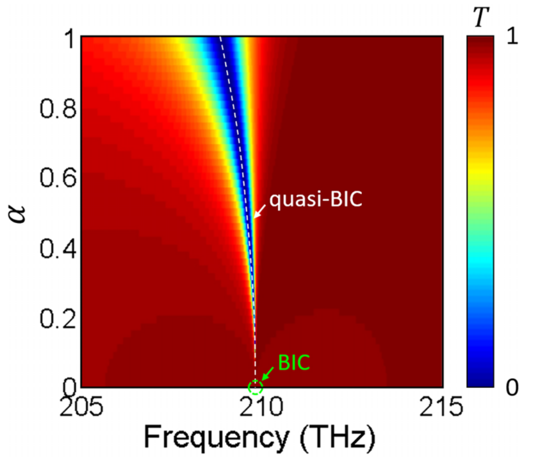

FIG. 3. TE transmittance spectrum of designed compound grating waveguide structure with varying geometric perturbation parameter α.

frequency, a Fano resonance occurs since the GMR condition is satisfied.

If the geometric perturbation parameter α changes from nonzero to zero, the previous excitable odd-order guided resonances (at points $P_{-1}, P_{-3}, \ldots$) turn into dark modes, i.e., BICs. In contrast, the even-order guided resonances (at points $P_{-2}, P_{-4}, \ldots$) are always excitable, giving rise to conventional Fano resonances. This mechanism to form BICs can be called selectable guided resonance.

To confirm the formation of the BIC, we calculate the TE transmittance spectrum of the designed compound grating waveguide structure with varying geometric perturbation parameter α based on the rigorous coupled-wave analysis (RCWA) [90,91], as shown in Fig. 3. The spatially modulated permittivity in the grating can be expanded into Fourier series as [67]

$$\varepsilon(x) = \sum_{m=-\infty}^{\infty} \varepsilon_m e^{i\frac{2m\pi x}{\Lambda}}, \tag{5a}$$

where the Fourier harmonics ε_m take the following forms:

$$\varepsilon_0 = 0.4n_{\mathrm{H}}^2 + 0.6n_{\mathrm{L}}^2, \tag{5b}$$

$$\varepsilon_m = \left(n_{\mathrm{H}}^2 - n_{\mathrm{L}}^2\right)\frac{\sin[m\pi(1-f_{\mathrm{L2}})] - \sin(m\pi f_{\mathrm{L1}})}{m\pi} \quad (m = \pm1,\ \pm2, \cdots). \tag{5c}$$

As the geometric perturbation parameter $\alpha = 1$, a Fano dip occurs at 208.84 THz. As the geometric perturbation parameter α gradually decreases, the resonant width of the Fano dip reduces dramatically. As the geometric perturbation parameter α continues to decrease to 0, the Fano dip completely disappears at 209.82 THz. From the results in Fig. 3, we can conclude that the quasi-BIC with finite resonant width turns into a BIC with vanishing resonant width as the geometric perturbation parameter α decreases from 1 to 0. The BIC frequency in transmittance spectrum (209.82 THz) slightly deviates from the BIC frequency predicted by the GMR theory ($f_{-1} = 209.9$ THz). The relative error is only 0.038%.

Next, we calculate the TE transmittance spectra of the designed compound grating waveguide structures for different geometric perturbation parameters $\alpha = 0.6,\ 0.4,\ 0.2$, and 0, as shown in Fig. 4(a). For better visuality, the transmittance curves are shifted in the unit of 1. The insets show the electric-field distributions ($|E_y|$) at the corresponding transmittance dips. The magnitude of the incident dielectric field is normalized, i.e., $|E_y| = 1$ V/m. As the geometric perturbation parameter $\alpha = 0.6$, a Fano dip occurs at 209.49 THz. Besides, the electric field is strongly localized inside the HfO_2 waveguide layer due to the GMR. As the geometric perturbation parameter α decreases from 0.6 to 0.2, the Fano dip slightly shifts towards higher frequencies and its resonant width reduces dramatically. Besides, the electric field inside the HfO_2 waveguide layer becomes stronger. As the geometric perturbation parameter α continues to decrease to 0, the Fano dip vanishes completely.

Using the eigensolver in COMSOL MULTIPHYSICS, we obtain the complex eigenfrequencies and Q factors of the eigenmodes for different geometric perturbation parameters, as given in Table I. The real parts of the complex eigenfrequencies of the eigenmodes agree well with the frequencies of the transmittance dips in the transmittance spectra calculated by the RCWA. Figure 4(b) further gives the dependence of the

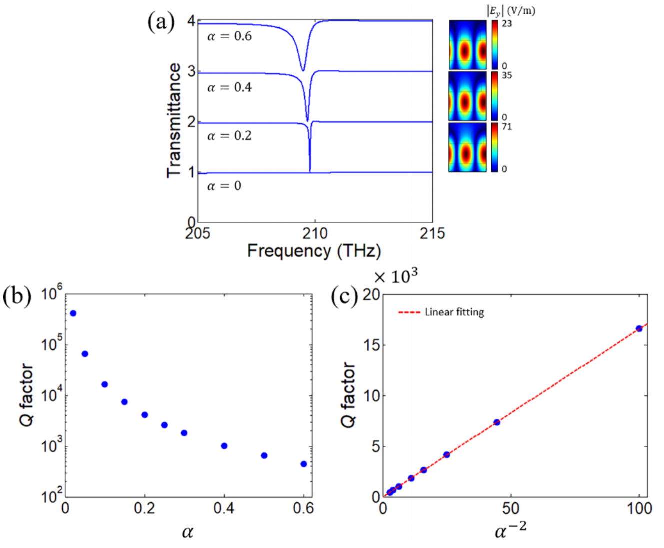

FIG. 4. (a) TE transmittance spectra of designed compound grating waveguide structures for different geometric perturbation parameters $\alpha = 0.6,\ 0.4,\ 0.2$, and 0. Insets show electric-field distributions ($|E_y|$) at corresponding transmittance dips. Magnitude of incident dielectric field is normalized, i.e., $|E_y| = 1$ V/m. (b) Dependence of Q factor of quasi-BIC on α. (c) Dependence of Q factor of quasi-BIC on α^{-2}. Red dashed line represents linear fitting curve.

TABLE I. Complex eigenfrequencies and Q factors of eigenmodes for different geometric perturbation parameters.

α	Complex eigenfrequency (THz)	Q factor
0.6	$209.37 + 2.3341\times10^{-1}i$	4.4850×10^{2}
0.5	$209.46 + 1.6076\times10^{-1}i$	6.5148×10^{2}
0.4	$209.54 + 1.0222\times10^{-1}i$	1.0249×10^{3}
0.3	$209.60 + 5.7215\times10^{-2}i$	1.8317×10^{3}
0.25	$209.62 + 3.9656\times10^{-2}i$	2.6430×10^{3}
0.2	$209.64 + 2.5340\times10^{-2}i$	4.1365×10^{3}
0.15	$209.66 + 1.4237\times10^{-2}i$	7.3631×10^{3}
0.1	$209.67 + 6.3222\times10^{-3}i$	1.6582×10^{4}
0.05	$209.67 + 1.5797\times10^{-3}i$	6.6362×10^{4}
0.02	$209.67 + 2.5274\times10^{-4}i$	4.1480×10^{5}

Q factor of the quasi-BIC on α. When $\alpha = 0.6$, the Q factor of the quasi-BIC is only 4.4850×10^{2}. As α approaches 0, the Q factor increases significantly. When $\alpha = 0.02$, the Q factor reaches 4.1480×10^{5}. When $\alpha = 0$, the Q factor becomes infinite. According to the perturbation theory in Ref. [59], the Q factor of the quasi-BIC is proportional to the negative quadratic power of the geometric perturbation parameter, i.e., $Q \propto \alpha^{-2}$. Note that $Q \propto \alpha^{-2}$ is only rigorously satisfied when α is small. In Fig. 4(c), we also give the dependence of the Q factor of the quasi-BIC on α^{-2}. We fit the data from $\alpha = 0.1$ to 0.6. The red dashed line represents the linear fitting curve. Clearly, the Q factor of the quasi-BIC is almost perfectly proportional to the negative quadratic power of the geometric perturbation parameter. The linear fitting curve takes the following form:

$$Q = 165.94\alpha^{-2} - 12.213. \tag{6}$$

Finally, we consider the intrinsic and scattering losses of HfO_2 in the fabrication process. By fitting the measured reflectance spectrum of the HfO_2-based grating structure in Ref. [92], the effective extinction coefficient of HfO_2 induced by the intrinsic and scattering losses can be obtained as $\kappa_{\mathrm{eff,H}} = 3\times10^{-5}$ (details can be seen in Sec. I of the Supplemental Material [93]). The refractive index of HfO_2 becomes $n_{\mathrm{H}} = n_{\mathrm{WG}} = 1.88 + 3\times10^{-5}i$. Figure 5(a) gives the dependence of the Q factor of the quasi-BIC on α. When $\alpha = 0.6$, the Q factor of the quasi-BIC is only 4.4288×10^{2}.

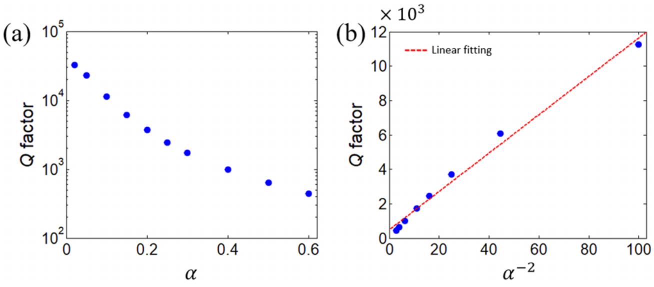

FIG. 5. (a) Dependence of Q factor of quasi-BIC on α. (b) Dependence of Q factor of quasi-BIC on α^{-2}. Red dashed line represents linear fitting curve. Refractive index of HfO_2 is set to be $n_{\mathrm{H}} = n_{\mathrm{WG}} = 1.88 + 3\times10^{-5}i$.

As α approaches 0, the Q factor increases significantly. When $\alpha = 0.02$, the Q factor reaches 3.2343×10^{5}. Also, we give the dependence of the Q factor of the quasi-BIC on α^{-2}, as shown in Fig. 5(b). We fit the data from $\alpha = 0.1$ to 0.6. The red dashed line represents the linear fitting curve. Owing to the absorption of HfO_2, the linear relationship between Q factor of the quasi-BIC and the negative quadratic power of the geometric perturbation parameter is slightly broken. The linear fitting curve takes the following form:

$$Q = 111.47\alpha^{-2} + 1009.4. \tag{7}$$

III. ULTRASLOW LIGHT EFFECT DRIVEN BY QUASI-BICS

Now, we explore the possibility to achieve ultraslow light effect driven by quasi-BICs. In Sec. III A, we give the theoretical model for calculating the group velocity of light. In Secs. III B and III C, we achieve ultraslow light effect driven by the quasi-BICs in lossless and lossy cases, respectively.

A. Theoretical model for calculating group velocity of light

It is known that the in-plane component of the group velocity of light can be calculated by the slope of the photonic band in the band structure [31]. For normal incident light, the in-plane component of the group velocity is zero since the slope of the photonic band is zero at the Γ point in the Brillouin zone (details can be seen in Sec. II of the Supplemental Material [93]). To calculate the out-of-plane component of the group velocity of light, we utilize an indirect method through the transmission coefficient [94–96]. According to Refs. [94–96], the out-of-plane component of the group velocity of light can be calculated by

$$v_g(\omega) = \frac{d\omega}{dk_z}. \tag{8}$$

The transmission coefficient of the compound grating waveguide structure can be further given by

$$t(\omega) = \mathrm{Re}[t(\omega)] + i\,\mathrm{Im}[t(\omega)] = |t(\omega)|e^{i\varphi(\omega)}. \tag{9}$$

In Eq. (9), $\varphi(\omega)$ represents the transmission phase of the compound grating waveguide structure, which can be expressed as

$$\varphi(\omega) = k_z(\omega)(d_{\mathrm{G}} + d_{\mathrm{WG}}). \tag{10}$$

According to Eqs. (9) and (10), we have

$$\tan[k_z(\omega)(d_{\mathrm{G}} + d_{\mathrm{WG}})] = \frac{\mathrm{Im}[t(\omega)]}{\mathrm{Re}[t(\omega)]}. \tag{11}$$

Differentiating both sides of Eq. (11) with respect to the angular frequency ω, we have

$$\{1 + \tan^2[k_z(\omega)(d_{\mathrm{G}} + d_{\mathrm{WG}})]\}(d_{\mathrm{G}} + d_{\mathrm{WG}})\frac{dk_z(\omega)}{d\omega} = \frac{\frac{d\{\mathrm{Im}[t(\omega)]\}}{d\omega}\mathrm{Re}[t(\omega)] - \frac{d\{\mathrm{Re}[t(\omega)]\}}{d\omega}\mathrm{Im}[t(\omega)]}{\{\mathrm{Re}[t(\omega)]\}^2}. \tag{12}$$

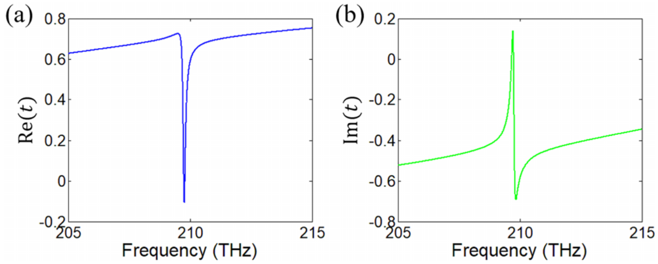

FIG. 6. (a) Real and (b) imaginary parts of transmission coefficient as functions of frequency.

Combining Eqs. (8), (11), and (12), we can obtain

$$v_g(\omega) = \frac{\{\mathrm{Re}[t(\omega)]\}^2 + \{\mathrm{Im}[t(\omega)]\}^2}{\frac{d\{\mathrm{Im}[t(\omega)]\}}{d\omega}\mathrm{Re}[t(\omega)] - \frac{d\{\mathrm{Re}[t(\omega)]\}}{d\omega}\mathrm{Im}[t(\omega)]}(d_{\mathrm{G}} + d_{\mathrm{WG}}). \tag{13}$$

B. Ultraslow light effect driven by quasi-BIC in lossless case

Considering the difficulty of the fabrication, we select the geometric perturbation parameter to be $\alpha = 0.3$. The widths of the two air grooves are $w_{\mathrm{L1}} = f_{\mathrm{L1}}\Lambda = 0.26\Lambda$ and $w_{\mathrm{L2}} = f_{\mathrm{L2}}\Lambda = 0.14\Lambda$, respectively. The width difference between the two air grooves is up to $\Delta w = w_{\mathrm{L1}} - w_{\mathrm{L2}} = 0.12\Lambda = 102$ nm, which is well within the reach of current fabrication technique [97]. Figures 6(a) and 6(b) give the real and imaginary parts of the transmission coefficient as functions of the frequency. Both the real and imaginary parts of the transmission coefficient change dramatically around the quasi-BIC frequency, while they change smoothly far away from the quasi-BIC frequency.

According to Eq. (13), we calculate the group velocity of light v_g as a function of the frequency, as shown in Fig. 7. The group velocity of light is in units of c. It should be noticed that the group velocity of light vanishes when $\mathrm{Re}[t(\omega)] = \mathrm{Im}[t(\omega)] = 0$. Therefore, this point should be avoided when calculating the group velocity of light. The result shows that the group velocity of light is intensively slowed down to $8.632\times10^{-4}c$ at the quasi-BIC frequency. Driven by the unique resonant property of the quasi-BIC in the compound grating waveguide structure, the group velocity of light can be intensively slowed down to the order of $10^{-4}c$.

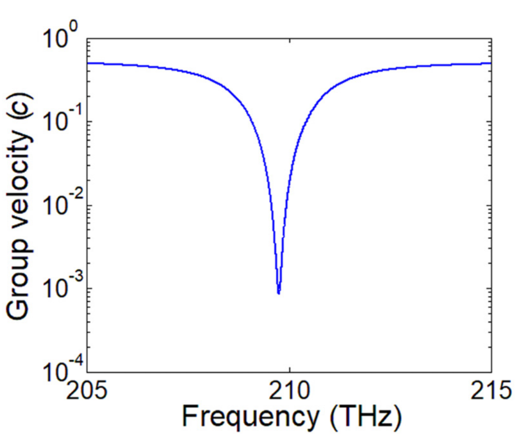

FIG. 7. Group velocity of light as function of frequency.

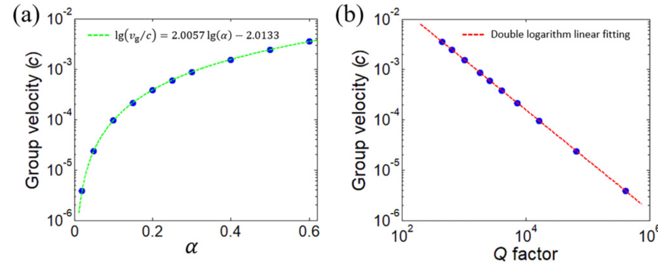

FIG. 8. (a) Dependence of group velocity of light on geometric perturbation parameter. Green dashed line represents double-logarithm linear fitting function $\lg(v_g/c) = 2.0057\,\lg(\alpha) - 2.0133$. (b) Dependence of group velocity of light on Q factor of quasi-BIC. Red dashed line represents double-logarithm linear fitting function.

Next, we calculate the dependence of the group velocity of light v_g on the geometric perturbation parameter α, as shown in Fig. 8(a). When $\alpha = 0.6$, the group velocity of light is $3.519\times10^{-3}c$. As α approaches 0, the group velocity of light decreases significantly. When $\alpha = 0.02$, the group velocity of light is intensively slowed down to $3.817\times10^{-6}c$. When $\alpha = 0$, the group velocity of light becomes infinitely low. The underlying reason is that a stronger resonance induces a stronger slow light effect. It is known that the Fabry-Perot resonance can enable slow light effect [98]. Nevertheless, the group velocity of light is finitely low since the Q factor of the Fabry-Perot resonance is finitely high. In Fig. 8(b), we further give the dependence of the group velocity of light v_g on the Q factor of the quasi-BIC. As shown by the red dashed line, the group velocity of light and Q factor of the quasi-BIC almost perfectly conform to double-logarithm linear relationship, i.e.,

$$\lg(v_g/c) = -0.999\,61\,\lg(Q) + 0.197\,66. \tag{14}$$

Under current fabrication technique, the measured Q factor of the quasi-BIC can reach the order of 10^4 to 10^6 [57,97,99]. Hence, it is possible to further slow down the group velocity of light to the order of $10^{-5}c$. As we discussed in Sec. II [see Fig. 4(c)], the Q factor of the quasi-BIC is almost perfectly proportional to the negative quadratic power of the geometric perturbation parameter,

$$Q = K\alpha^{-2}, \tag{15}$$

where $K > 0$ is the proportionality factor. Taking the logarithm of both sides of Eq. (15), we can obtain

$$\lg(Q) = -2\,\lg(\alpha) + K', \tag{16}$$

where $K' = \lg(K)$. Combining Eqs. (14) and (16), the group velocity of light v_g and geometric perturbation parameter α also conforms to double-logarithm linear relationship. Therefore, we utilize a double-logarithm linear function to fit the data of the group velocity of light v_g and geometric perturbation parameter α in Fig. 8(a). As shown by the green dashed line, the fitting double-logarithm linear function can be expressed as

$$\lg(v_g/c) = 2.0057\,\lg(\alpha) - 2.0133. \tag{17}$$

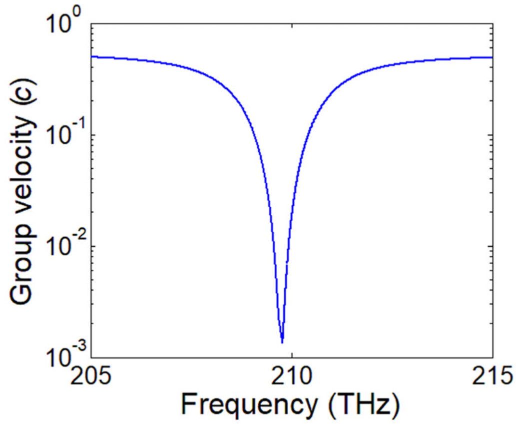

FIG. 9. Group velocity of light as function of frequency. Refractive index of HfO_2 is set to be $n_H = n_{WG} = 1.88 + 3\times10^{-5}i$.

Notice that the coefficient of the term $\lg(\alpha)$ slightly derives from $(-0.999\,61)\times(-2) = 1.999\,22$ since the relationship $Q = K\alpha^{-2}$ is not satisfied rigorously [see Eq. (6)]. As demonstrated, the fitting curve agrees well with the data. By solving Eq. (17), we can finally obtain the relationship between the group velocity of light v_g and geometric perturbation parameter α:

$$v_g = 0.009\,698\,4\times10^{2.0057\ \lg(\alpha)}c. \tag{18}$$

It should be noted that when the parameters (such as the period and thickness of the grating layer, the filling ratio of HfO_2 ridge, and the thickness of the waveguide layer) change, the double-logarithm linear relationship between the group velocity of light and geometric perturbation parameter can still be satisfied (details can be seen in Sec. III of the Supplemental Material [93]). The only difference is the values of two coefficients.

C. Ultraslow light effect driven by quasi-BIC in lossy case

Finally, we discuss the ultraslow light effect driven by the quasi-BIC in lossy case. As we discussed in Sec. II, the refractive index of HfO_2 is set to be $n_H = n_{WG} = 1.88 + 3\times10^{-5}i$. Figure 9 gives the group velocity of light as a function of the frequency, respectively. The result shows that the group velocity of light is intensively slowed down to $1.316\times10^{-3}c$ at the quasi-BIC frequency. When considering the intrinsic and scattering losses of HfO_2 in the fabrication process, the group velocity of light can still be intensively slowed down to the order of $10^{-3}c$.

Figure 10(a) gives the dependence of the group velocity of light v_g on the geometric perturbation parameter α. When $\alpha = 0.6$, the group velocity of light is $4.108\times10^{-3}c$. As α approaches 0, the group velocity of light decreases significantly. When $\alpha = 0.1$, the group velocity of light is intensively slowed down to $5.558\times10^{-4}c$. In Fig. 10(b), we further give the dependence of the group velocity of light v_g on the Q factor of the quasi-BIC. As shown by the red dashed line, the group velocity of light and Q factor of the quasi-BIC approximately conforms to double-logarithm linear relationship, i.e.,

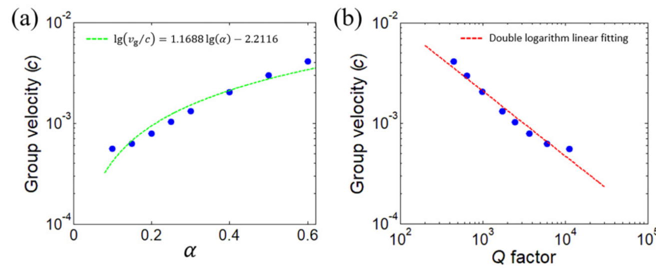

FIG. 10. (a) Dependence of group velocity of light on geometric perturbation parameter. Green dashed line represents double-logarithm linear fitting function $\lg(v_g/c) = 1.1688\ \lg(\alpha) - 2.2116$. (b) Dependence of group velocity of light on Q factor of quasi-BIC. Red dashed line represents double-logarithm linear fitting function. Refractive index of HfO_2 is set to be $n_H = n_{WG} = 1.88 + 3\times10^{-5}i$.

$$\lg(v_g/c) = -0.646\,58\ \lg(Q) - 0.738\,46. \tag{19}$$

Owing to the absorption of HfO_2, the double-logarithm linear relationship between the group velocity of light and Q factor of the quasi-BIC is slightly broken. Similar to Sec. III B, we utilize a double-logarithm linear function to fit the data of the group velocity of light v_g and geometric perturbation parameter α in Fig. 10(a). As shown by the green dashed line, the fitting double-logarithm linear function can be expressed as

$$\lg(v_g/c) = 1.1688\ \lg(\alpha) - 2.2116. \tag{20}$$

As demonstrated, the fitting curve approximately agrees with the data. Owing to the absorption of HfO_2, the double-logarithm linear relationship between the group velocity of light and geometric perturbation parameter is slightly broken. By solving Eq. (20), we can finally obtain the relationship between the group velocity of light v_g and geometric perturbation parameter α:

$$v_g = 0.006\,143\,3\times10^{1.1688\ \lg(\alpha)}c. \tag{21}$$

IV. CONCLUSIONS

In summary, we achieve ultraslow light effect driven by the quasi-BICs in a compound grating waveguide structure with a complex lattice. Empowered by the unique resonant property of the quasi-BICs, the group velocity of light can be intensively slowed down. Then, we disclose that the group velocity of light and geometric perturbation parameters conforms to double-logarithm linear relationship. Our findings not only offer unique insight for the relation between slow light effect and BIC, but also provide a viable route to designing high-performance slow light-based optical devices.

ACKNOWLEDGMENTS

This work is sponsored by the National Natural Science Foundation of China (Grants No. 12104105, No. 12364045, No. 12304420, and No. 12264028), the

Guangdong Basic and Applied Basic Research Foundation (Grant No. 2023A1515011024), the Science and Technology Program of Guangzhou (Grant No. 202201011176), the Natural Science Foundation of Jiangxi Province (Grants No. 20232BAB211025 and No. 20232BAB201040), the China Scholarship Council (Grant No. 202008420045), and the Start-up Funding of Guangdong Polytechnic Normal University (Grant No. 2021SDKYA033). F.W. would like to think Dr. Yang Long from Nanyang Technological University for the helpful discussion on the calculation of group velocity.

[1] M. Born and E. Wolf, *Principles of Optics: Electromagnetic Theory of Propagation, Interference and Diffraction of Light*, 6th ed. (Pergamon Press, Oxford, 1980).

[2] J. Weiner and P.-T. Ho, *Light-matter Interactions: Fundamentals and Applications* (Wiley, New York, 2003).

[3] E. Viasnoff-Schwoob, C. Weisbuch, H. Benisty, S. Olivier, S. Varoutsis, I. Robert-Philip, R. Houdré, and C. J. M. Smith, Spontaneous emission enhancement of quantum dots in a photonic crystal wire, Phys. Rev. Lett. **95**, 183901 (2005).

[4] M. Gupta, Y. K. Srivastava, M. Manjappa, and R. Singh, Sensing with toroidal metamaterial, Appl. Phys. Lett. **110**, 121108 (2017).

[5] S. Karmakar, D. Kumar, R. K. Varshney, and D. R. Chowdhury, Strong terahertz matter interaction induced ultrasensitive sensing in Fano cavity based stacked metamaterials, J. Phys. D: Appl. Phys. **53**, 415101 (2020).

[6] G. Günter, A. A. Anappara, J. Hees, A. Sell, G. Biasiol, L. Sorba, S. De Liberato, C. Ciuti, A. Tredicucci, A. Leitenstorfer, and R. Huber, Sub-cycle switch-on of ultrastrong light-matter interaction, Nature (London) **458**, 178 (2009).

[7] G. Chen, Y.-C. Yu, X.-L. Zhuo, Y.-G. Huang, H. Jiang, J.-F. Liu, C.-J. Jin, and X.-H. Wang, Ab initio determination of local coupling interaction in arbitrary nanostructures: Application to photonic crystals and cavities, Phys. Rev. B **87**, 195138 (2013).

[8] Y. Ashida, A. İmamoğlu, and E. Demler, Cavity quantum electrodynamics at arbitrary light-matter coupling strengths, Phys. Rev. Lett. **126**, 153603 (2021).

[9] N. Rivera and I. Kaminer, Light-matter interactions with photonic quasiparticles, Nat. Rev. Phys. **2**, 538 (2020).

[10] M. Soljačić, S. G. Johnson, S. Fan, M. Ibanescu, E. Ippen, and J. D. Joannopoulos, Photonic-crystal slow-light enhancement of nonlinear phase sensitivity, J. Opt. Soc. Am. B **19**, 2052 (2002).

[11] Y. A. Vlasov, M. O'Boyle, H. F. Hamann, and S. J. McNab, Active control of slow light on a chip with photonic crystal waveguides, Nature (London) **438**, 65 (2005).

[12] T. F. Krauss, Slow light in photonic crystal waveguides, J. Phys. D: Appl. Phys. **40**, 2666 (2007).

[13] T. Baba, Slow light in photonic crystals, Nat. Photon. **2**, 465 (2008).

[14] M. C. Muñoz, A. Yu. Petrov, L. O'Faolain, J. Li, T. F. Krauss, and M. Eich, Optical induced indirect photonic transitions in a slow light photonic crystal waveguide, Phys. Rev. Lett. **112**, 053904 (2014).

[15] L. V. Hau, S. E. Harris, Z. Dutton, and C. H. Behroozi, Light speed reduction to 17 metres per second in an ultracold atonic gas, Nature (London) **397**, 594 (1999).

[16] D. A. Braje, V. Balić, G. Y. Yin, and S. E. Harris, Low-light-level nonlinear optics with slow light, Phys. Rev. A **68**, 041801(R) (2003).

[17] H. Kang, G. Hernandez, and Y. Zhu, Superluminal and slow light propagation in cold atoms, Phys. Rev. A **70**, 011801(R) (2004).

[18] I. Novikova, D. F. Philips, and R. L. Walsworth, Slow light with integrated gain and large pulse delay, Phys Rev. Lett. **99**, 173604 (2007).

[19] A. Tyszka-Zawadzka, B. Janaszek, and P. Szczepański, Tunable slow light in graphene-based hyperbolic metamaterial waveguide operating in SCLU telecom bands, Opt. Express **25**, 7263 (2017).

[20] V. B. Novikov, A. P. Leontiev, K. S. Napolskii, and T. V. Murzina, Nonlocality-driven switchable fast-slow light effect in hyperbolic metamaterials in epsilon-near-zero regime, Phys. Rev. B **106**, 165415 (2022).

[21] M. Soljačić and J. D. Joannopoulos, Enhancement of nonlinear effects using photonic crystals, Nat. Mater. **3**, 211 (2004).

[22] R. S. Jacobsen, K. N. Andersen, P. I. Borel, J. Fage-Pedersen, L. H. Frandsen, O. Hansen, M. Kristensen, A. V. Lavrinenko, G. Moulin, H. Ou, C. Peucheret, B. Zsigri, and A. Bjarklev, Strained silicon as a new electro-optic material, Nature (London) **441**, 199 (2006).

[23] C. Yu, T. Luo, L. Zhang, and A. E. Willner, Data pulse distortion induced by a slow-light tunable delay line in optical fiber, Opt. Lett. **32**, 20 (2007).

[24] D. M. Beggs, I. H. Rey, T. Kampfrath, N. Rotenberg, L. Kuiers, and T. F. Krauss, Ultrafast tunable optical delay line based on indirect photonic transitions, Phys. Rev. Lett. **108**, 213901 (2012).

[25] M. Bajcsy, S. Hofferberth, V. Balic, T. Peyronel, M. Hafezi, A. S. Zibrov, V. Vuletic, and M. D. Lukin, Efficient all-optical switching using slow light within a hollow fiber, Phys. Rev. Lett. **102**, 203902 (2009).

[26] L. Torrijos-Morán, A. Brimont, A. Griol, P. Sanchis, and J. García-Rupérez, Ultra-compact optical switches using slow light bimodal silicon waveguides, J. Lightwave Technol. **39**, 3495 (2021).

[27] R. S. Tucker, P.-C. Ku, and C. J. Chang-Hasnain, Slow-light optical buffers: Capabilities and fundamental limitations, J. Lightwave Technol. **23**, 4046 (2005).

[28] S.-Y. Lin, J. G. Fleming, and I. El-Kady, Experimental observation of photonic-crystal emission near a photonic band edge, Appl. Phys. Lett. **83**, 593 (2003).

[29] J. Grgić, S. Xiao, J. Mørk, A. Jauho, and N. A. Mortensen, Slow-light enhanced absorption in a hollow-core fiber, Opt. Express **18**, 14270 (2010).

[30] B. Corcoran, C. Monat, C. Grillet, D. J. Moss, B. J. Eggleton, T. P. White, L. O'Faolain, and T. F. Krauss, Green light emission in silicon through slow-light enhanced third-harmonic generation in photonic-crystal waveguides, Nat. Photon. **3**, 206 (2009).

[31] H. Gersen, T. J. Karle, R. J. P. Engelen, W. Bogaerts, J. P. Korterik, N. F. van Hulst, T. F. Krauss, and L. Kuipers, Real-Space observation of ultraslow light in photonic crystal waveguides, Phys. Rev. Lett. **94**, 073903 (2005).

[32] M. L. Povinelli, S. G. Johnson, and J. D. Joannopoulos, Slow-light, band-edge waveguides for tunable time delays, Opt. Express **13**, 7145 (2005).
[33] S. Mookherjea, J. S. Park, S.-H. Yang, and P. R. Bandaru, Localization in silicon nanophotonic slow-light waveguides, Nat. Photon. **2**, 90 (2008).
[34] J. G. Pedersen, S. Xiao, and N. A. Mortensen, Limits of slow light in photonic crystals, Phys. Rev. B **78**, 153101 (2008).
[35] N. L. Thomas, H. Zhang, J. Jágerská, V. Zabelin, R. Houdré, I. Sagnes, and A. Talneau, Light transport regimes in slow light photonic crystal waveguides, Phys. Rev. B **80**, 125332 (2009).
[36] C. Kraeh, J. L. Martinez-Hurtado, A. Popescu, H. Hedler, and J. J. Finley, Slow light enhanced gas sensing in photonic crystals, Opt. Mater. **76**, 106 (2018).
[37] V. Yannopapas, E. Paspalakis, and N. V. Vitanov, Electromagnetically induced transparency and slow light in an array of metallic nanoparticles, Phys. Rev. B **80**, 035104 (2009).
[38] A. H. Safavi-Naeini, T. P. M. Aleger, J. Chan, M. Eichenfield, M. Winger, Q. Lin, J. T. Hill, D. E. Chang, and O. Painter, Electromagnetically induced transparency and slow light with optomechanics, Nature (London) **472**, 69 (2011).
[39] I. Novikova, R. L. Walsworth, and Y. Xiao, Electromagnetically induced transparency-based slow and stored light in warm atoms, Laser Photon. Rev. **6**, 333 (2012).
[40] K. Zhang, C. Wang, L. Qin, R.-W. Peng, D.-H. Xu, X. Xiong, and M. Wang, Dual-mode electromagnetically induced transparency and slow light in a terahertz metamaterial, Opt. Lett. **39**, 3539 (2014).
[41] G. Lai, R. Liang, Y. Zhang, Z. Bian, L. Yi, G. Zhan, and R. Zhao, Double plasmonic nanodisks design for electromagnetically induced transparency and slow light, Opt. Express **23**, 6554 (2015).
[42] Z. Liao, Q. Ma, L. Wang, Z. Yang, M. Li, F. Deng, and W. Hong, Guiding-mode-assisted double-BICs in an all-dielectric metasurface, Opt. Express **30**, 24676 (2022).
[43] Z. Zhao, H. Zhao, R. T. Ako, S. Nickl, and S. Sriram, Polarization-insensitive terahertz spoof localized surface plasmon-induced transparency based on lattice rotational symmetry, Appl. Phys. Lett. **117**, 011105 (2020).
[44] Z. Zhao, Z. Gu, R. T. Ako, H. Zhao, and S. Sriram, Coherently controllable terahertz plasmon-induced transparency using a coupled Fano-Lorentzian metasurface, Opt. Express **28**, 15573 (2020).
[45] C. Xiong, H. Xu, M. Zhao, B. Zhang, C. Lui, B. Zeng, K. Wu, B. Ruan, M. Li, and H. Li, Triple plasmon-induced transparency and outstanding slow-light in quasi-continuous monolayer graphene structure, Sci. China Phys. Mech. **64**, 224211 (2021).
[46] P. Palinginis, F. Sedgwick, S. Crankshaw, M. Moewe, and C. J. Chang-Hasnain, Room temperature slow light in a quantum-well waveguide via coherent population oscillation, Opt. Express **13**, 9909 (2005).
[47] Z. Zhu, D. J. Gauthier, Y. Okawachi, J. E. Sharping, A. L. Gaeta, R. W. Boyd, and A. E. Willner, Numerical study of all-optical slow-light delays via simulated Brillouin scattering in an optical fiber, J. Opt. Soc. Am. B **22**, 2378 (2005).
[48] J. Q. Liang, M. Katsuragawa, F. Le Kien, and K. Hakuta, Slow light produced by simulated Raman scattering in solid hydrogen, Phys. Rev. A **65**, 031801(R) (2002).
[49] L. H. Frandsen, A. V. Lavinenko, J. Fage-Pederson, and P. I. Borel, Photonic crystal waveguides with semi-low light and tailored dispersion properties, Opt. Express **14**, 9444 (2006).
[50] S. Yan, X. Zhu, L. H. Frandsen, S. Xiao, N. A. Mortensen, J. Dong, and Y. Ding, Slow-light-enhanced energy efficiency for graphene microheaters on silicon photonic crystal waveguides, Nat. Commun. **8**, 14411 (2017).
[51] C. W. Hsu, B. Zhen, A. D. Stone, J. D. Joannopoulos, and M. Soljačić, Bound state in the continuum, Nat. Rev. Mater. **1**, 16048 (2016).
[52] A. A. Bogdanov, K. L. Koshelev, P. V. Kapitanova, M. V. Rybin, S. A. Gladyshev, Z. F. Sadrieva, K. B. Samusev, Y. S. Kivshar, and M. F. Limonov, Bound states in the continuum and Fano resonances in the strong mode coupling regime, Adv. Photon. **1**, 016001 (2019).
[53] S. Joseph, S. Pandey, S. Sarkar, and J. Joseph, Bound states in the continuum in resonant nanostructures: An overview of engineered materials for tailored applications, Nanophotonics **10**, 4175 (2021).
[54] S. I. Azzam and A. V. Kildishev, Photonic bound states in the continuum: From basics to applications, Adv. Opt. Mater. **9**, 2001469 (2021).
[55] A. F. Sadreev, Interference traps waves in an open system: Bound states in the continuum, Rep. Prog. Phys. **84**, 055901 (2021).
[56] C. W. Hsu, B. Zhen, J. Lee, S. Chua, S. G. Johnson, J. D. Joannopoulos, and M. Soljačić, Observation of trapped light within the radiation continuum, Nature (London) **499**, 188 (2013).
[57] J. Jin, X. Yin, L. Ni, M. Soljačić, B. Zhen, and C. Peng, Topologically enabled ultrahigh-Q guided resonances robust to out-of-plane scattering, Nature (London) **574**, 501 (2019).
[58] P. Hu, J. Wang, Q. Jiang, J. Wang, L. Shi, D. Han, Z. Q. Zhang, C. T. Chan, and J. Zi, Global phase diagram of bound states in the continuum, Optica **9**, 1353 (2022).
[59] K. Koshelev, S. Lepeshov, M. Liu, A. Bogdanov, and Y. Kivshar, Asymmetric metasurfaces with high-Q resonances governed by bound states in the continuum, Phys. Rev. Lett. **121**, 193903 (2018).
[60] J. Li, J. Li, C. Zheng, Z. Yue, D. Yang, S. Wang, M. Li, Y. Zhang, and J. Yao, Spectral amplitude modulation and dynamic near-field displaying of all-silicon terahertz metasurfaces supporting bound states in the continuum, Appl. Phys. Lett. **119**, 241105 (2021).
[61] S. Xiao, M. Qin, J. Duan, F. Wu, and T. Liu, Polarization-controlled dynamically switchable high-harmonic generation from all-dielectric metasurfaces governed by dual bound states in the continuum, Phys. Rev. B **105**, 195440 (2022).
[62] Y. Gao, L. Xu, and X. Shen, Q-factor mediated quasi-BIC resonances coupling in asymmetric dimer lattices, Opt. Express **30**, 46680 (2022).
[63] J. Wang, L. Shi, and J. Zi, Spin Hall effect of light via momentum-space topological vortices around bound states in the continuum, Phys. Rev. Lett. **129**, 236101 (2022).

[64] W. Wang, Y. K. Srivastava, T. C. Tan, Z. Wang, and R. Singh, Brillouin zone folding driven bound states in the continuum, Nat. Commun. **14**, 2811 (2023).
[65] J. Zhang, Y. Ruan, Z.-D. Hu, J. Wu, and J. Wang, An enhanced high Q-factor resonance of quasi-bound states in the continuum with all-dielectric metasurface based on multilayer film structures, IEEE Sensors **23**, 2070 (2023).
[66] D. C. Marinica and A. G. Borisov, Bound states in the continuum in photonics, Phys. Rev. Lett. **100**, 183902 (2008).
[67] W. Liu, Y. Li, H. Jiang, Z. Lai, and H. Chen, Controlling the spectral width in compound waveguide grating structures, Opt. Lett. **38**, 163 (2013).
[68] H. M. Doeleman, F. Monticone, W. den Hollander, A. Alù, and A. F. Koenderink, Experimental observation of a polarization vortex at an optical bound state in the continuum, Nat. Photon. **12**, 397 (2018).
[69] A. C. Overvig, S. Shrestha, and N. Yu, Dimerized high contrast gratings, Nanophotonics **7**, 1157 (2018).
[70] D. N. Maksimov, A. A. Bogdanov, and E. N. Bulgakov, Optical bistability with bound states in the continuum in dielectric gratings, Phys. Rev. A **102**, 033511 (2020).
[71] I. A. M. Al-Ani, K. As'Ham, L. Huang, A. E. Miroshnichenko, and H. T. Hattori, Enhanced strong coupling of TMDC monolayers by bound state in the continuum, Laser Photon. Rev. **15**, 2100240 (2021).
[72] F. Wu, D. Liu, and S. Xiao, Bandwidth-tunable near-infrared perfect absorption of graphene in a compound grating waveguide structure supporting quasi-bound states in the continuum, Opt. Express **29**, 41975 (2021).
[73] X. Liu, C. Zhang, J. Hu, and H. Han, Dual-band refractive index sensors with cascaded asymmetric resonant compound grating based on bound states in the continuum, Opt. Express **31**, 13959 (2023).
[74] K. Sun, H. Wei, W. Chen, Y. Chen, Y. Cai, C.-W. Qiu, and Z. Han, Infinite-Q guided modes radiate in the continuum, Phys. Rev. B **107**, 115415 (2023).
[75] F. Wu, J. Wu, Z. Guo, H. Jiang, Y. Sun, Y. Li, J. Ren, and H. Chen, Giant enhancement of the Goos-Hänchen shift assisted by quasibound states in the continuum, Phys. Rev. Appl. **12**, 014028 (2019).
[76] F. Wu, M. Luo, J. Wu, C. Fan, X. Qi, Y. Jian, D. Liu, S. Xiao, G. Chen, H. Jiang, Y. Sun, and H. Chen, Dual quasi-bound states in the continuum in compound grating waveguide structures for large positive and negative Goos-Hänchen shifts with perfect reflection, Phys. Rev. A **104**, 023518 (2021).
[77] F. Wu, T. Liu, Y. Long, S. Xiao, and G. Chen, Giant photonic spin Hall effect empowered by polarization-dependent quasi-bound states in the continuum in compound grating waveguide structures, Phys. Rev. B **107**, 165428 (2023).
[78] J. Liu, C. Chen, X. Li, J. Li, D. Dong, Y. Liu, and Y. Fu, Tunable dual quasi-bound states in continuum and electromagnetically induced transparency enabled by the broken material symmetry in all-dielectric compound gratings, Opt. Express **31**, 4347 (2023).
[79] Y. Ruan, Z.-D. Hu, J. Wang, L. Yu, and Y. Wang, Adjacent asymmetric tilt grating structure with strong resonance assisted by quasi-bound states in the continuum, IEEE Photon. J. **14**, 4655906 (2022).
[80] S. Chen, Z. Li, Y. Mao, X. Dai, and Y. Xiang, Giant enhancement of the Goos-Hänchen shift assisted by merging bound states in the continuum, J. Appl. Phys. **133**, 193101 (2023).
[81] S. S. Biswas, G. Remesh, V. G. Achanta, A. Banerjee, N. Ghosh, and S. D. Gupta, Enhanced beam shifts mediated by bound states in continuum, J. Opt. **25**, 095401 (2023).
[82] T. Ning, X. Li, Y. Zhao, L. Yin, Y. Huo, L. Zhao, and Q. Yue, Giant enhancement of harmonic generation in all-dielectric resonant waveguide gratings of quasibound states in the continuum, Opt. Express **28**, 34024 (2020).
[83] Z. Huang, M. Wang, Y. Li, J. Shang, K. Li, W. Qiu, J. Dong, H. Guan, Z. Chen, and H. Lu, Highly efficient second harmonic generation of thin film lithium niobate nanograting near bound states in the continuum, Nanotechnology **32**, 325207 (2021).
[84] X. Li, D. Liu, Y. Huo, Q. Yue, and T. Ning, Low-voltage electro-optic switching and modulation of second harmonic generation in lithium niobate resonant waveguide gratings assisted by quasi-BICs, Opt. Laser Technol. **160**, 109083 (2023).
[85] X. Li, Z. Zhang, Y. Huo, L. Zhao, Q. Yue, S. Jiang, H. Liang, Y. Gao, and T. Ning, Broadband and ultra-low threshold optical bistability in guided-mode resonance grating nanostructures of quasi-bound states in the continuum, Nanomaterials **11**, 2843 (2021).
[86] M. F. Al-Kuhaili, Optical properties of hafnium oxide thin films and their applications in energy-efficient windows, Opt. Mater. **27**, 383 (2004).
[87] E. Palik, *Handbook of Optical Constants of Solids I* (Academic Press, New York, 1985).
[88] T. Sang, S. Cai, and Z. Wang, Guided-mode resonance filter with an antireflective surface consisting of a buffer layer with refractive index equal to that of the grating, J. Mod. Opt. **58**, 1260 (2011).
[89] A. Yariv and P. Yeh, *Optical Waves in Crystals* (Wiley, New York, 1984).
[90] M. G. Moharam, D. A. Pommet, E. B. Grann, and T. K. Gaylord, Stable implementation of the rigorous coupled-wave analysis for surface-relief gratings: Enhanced transmittance matrix approach, J. Opt. Soc. Am. A **12**, 1077 (1995).
[91] F. Li, Use of Fourier series in the analysis of discontinuous periodic structures, J. Opt. Soc. Am. A **13**, 1870 (1996).
[92] Z. S. Liu, S. Tibuleac, D. Shin, P. P. Young, and R. Magnusson, High-efficiency guided-mode resonance filter, Opt. Lett. **23**, 1556 (1998).
[93] See Supplemental Material at http://link.aps.org/supplemental/10.1103/PhysRevB.108.165404 for the effective extinction coefficient of HfO_2 in the HfO_2-based grating structure; the photonic band of the quasi-BIC for the geometric perturbation parameter $\alpha = 0.3$; the double logarithm linear relationship between the group velocity of light and geometric perturbation parameter in other cases.
[94] J. M. Bendickson, J. P. Dowling, and M. Scalora, Analytic expressions for the electromagnetic mode density in finite, one-dimensional, photonic band-gap structures, Phys. Rev. E **53**, 4107 (1996).
[95] A. H. Gevorgyan, K. B. Oganesyan, G. A. Vardanyan, and G. K. Matinyan, Photonic density of states of cholesteric liquid crystal cells, Laser Phys. **24**, 115801 (2014).

[96] B. Janaszek, A. Tyazka-Zawadzka, and P. Szczepański, Dispersion-enabled control of photonic density of states in photonic hypercrystals, Opt. Express **31**, 27948 (2023).
[97] Z. Liu, Y. Xu, Y. Lin, J. Xiang, T. Feng, Q. Cao, J. Li, S. Lan, and J. Liu, High-Q quasibound states in the continuum for nonlinear metasurfaces, Phys. Rev. Lett. **123**, 253901 (2019).
[98] A. Yariv and P. Yeh, *Photonics: Optical Electronics in Modern Communications*, 6th ed. (Oxford University Press, New York, 2006).
[99] Z. Chen, X. Yin, J. Jin, Z. Zheng, Z. Zhang, F. Wang, L. He, B. Zhen, and C. Peng, Observation of miniaturized bound states in the continuum with ultra-high quality factors, Sci. Bull. **67**, 359 (2022).